

The ground states and spin textures of rotating two-component Bose–Einstein condensates in an annular trap

Jingjing Jin, Suying Zhang¹, Wei Han and Zhifeng Wei

Institute of Theoretical Physics, Shanxi University, Taiyuan 030006, People's Republic of China

E-mail: zhangsy@sxu.edu.cn

Received 7 January 2013, in final form 17 February 2013

Published 13 March 2013

Online at stacks.iop.org/JPhysB/46/075302

Abstract

We investigate the ground states and spin textures of rotating two-component Bose–Einstein condensates (BECs) confined in an annular potential. For the two-component miscible BECs, we analytically give the critical angular velocity of each component with the Thomas–Fermi approximation (TFA), at which the density profile changes from a disc shape into an annulus shape, forming a giant vortex. We present a phase diagram showing three kinds of density profiles of the ground states that are two disc shaped, one disc and another annulus shaped, and two annulus shaped. For the two-component immiscible BECs with particle number grave imbalance, we also discuss their ground states using the TFA, and three kinds of symmetrical structures of the density profiles are classified analytically. The spin textures of the two-component immiscible BECs have been studied and we find three kinds of symmetrical structures of the spin textures in the annular trap. One of these textures is an annular skyrmion which has been observed in harmonic potentials. Both of the other spin textures contain a new structure composed of concentric double-annulus skyrmion whose topological charge is the sum of the ones of two annular skyrmions, and the topological charge of each annular skyrmion is equal to the absolute value of the difference between the quantum numbers of circulation of two components inside this annular skyrmion. We also prove that these new textures are robust by investigating the dynamical behaviours of the system under external disturbances.

(Some figures may appear in colour only in the online journal)

1. Introduction

In recent years, many interesting consequences have been obtained theoretically and experimentally in the field of cold atoms. With the improved experimental technology, it is very easy to construct and control different structures of potentials such as the harmonic potentials, the optical lattice potentials and the annular or ring-shaped potentials [1–4]. Because of the circular geometric structure, the annular potentials are very important for many fields, such as the accelerator physics [5–8], persistent currents [2], vortices [9, 10], solitons [11–13] in Bose–Einstein condensates (BECs) and so on.

The rotating single-component BECs in anharmonic trapping potentials have been studied extensively and display

very rich topological states with unique vortex structures [14, 15]. Many theoretical studies about two-component BECs confined in annular traps have been carried out. For example, the rotational properties of two-component Bose gases confined in a one-dimensional single-ring potential are studied and the persistent currents are found in this system [16]. And various phases of the ground state are identified and the rotational properties are also studied for the mixture of Bose gases confined in a two-dimensional concentric double-annulus-like trap [17]. However, few researches about the vortex structures have been carried out and none of these studies has considered the spin textures of the rotating two-component BECs in a two-dimensional annular trap.

In this paper, we investigate the ground states and the spin textures of rotating two-component BECs confined in a two-dimensional annular trap. The system has many parameters

¹ Author to whom any correspondence should be addressed.

such as anharmonic trapping potential, rotation angular velocity, population imbalance between the two components, inter-component and intra-component interaction strengths, and the interplay of them will induce a very rich phase diagram. Firstly, we consider the ground states of two miscible components with different angular velocities. For each component, a central density hole which contains several phase defects will appear, forming a giant vortex, when the angular velocity exceeds a critical value. We give their critical angular velocities with the Thomas–Fermi approximation (TFA) and present a phase diagram of the two components which shows three kinds of density profiles of the ground states by varying the angular velocities and intra-component interaction strengths.

Secondly, we study the ground states of two-component immiscible BECs with symmetric structures. For the two components with their particle number grave imbalance, the density distribution of the big component is hardly affected by the small one, but the small component experiences a trap formed by the external trap plus the repulsive interaction from the big component. So we can also approximate their profiles with the TFA, and the phases of the ground states are analytically classified into three kinds of symmetric structures according to the competition among the chemical potentials and the effective potential barriers. We also research numerically the spin textures of two-component immiscible BECs. Three kinds of interesting spin textures are found. One of them is annular skyrmion (giant skyrmion); this structure has been observed and researched in the harmonic trapping potentials [18, 19]. Both of the other spin textures contain a new structure which we name as concentric double-annulus skyrmion. This texture cannot exist in harmonic trapping potentials and has, so far, not been studied.

This paper is organized as follows: in section 2, we introduce the basic formulation of the problem. In section 3, the two-component miscible condensates are studied analytically with the TFA, and the phases of the ground states are classified. In section 4, we analytically discuss the two-component immiscible BECs with the TFA in the limit of $N_1 \gg N_2$. The density profiles and spin textures of the condensates in the annular trap are studied numerically. And the conclusions are given in section 5.

2. Formulation of the problem

We consider two-component BECs at zero temperature, confined in an axially symmetric potential:

$$V = \frac{1}{2}m[\omega_{\perp}^2 V_0(r - r_0)^2 + \omega_z^2 z^2], \quad (1)$$

where $r = \sqrt{x^2 + y^2}$, ω_{\perp} and ω_z are the frequencies of the confinement in the x - y plane and along the z axis, respectively. V_0 is a dimensionless constant that characterizes the barrier height for a fixed r_0 . The potential has a minimum at r_0 . Supposing $\lambda = \frac{\omega_z}{\omega_{\perp}} \gg 1$, the system can be simplified into a quasi-two-dimensional model, and the trapping potential is reduced to its two-dimensional form $V = \frac{1}{2}m\omega_{\perp}^2 V_0(r - r_0)^2$, as shown in figure 1. The trapped two-component BECs can be characterized by the condensate wavefunctions $\Psi =$

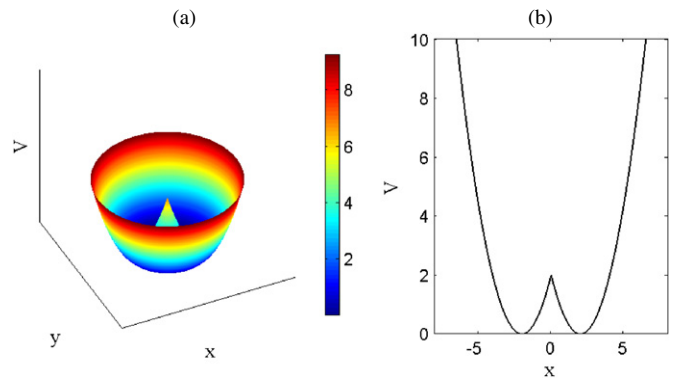


Figure 1. (a) Schematic of the annular trapping potential. (b) The cross sections of V along the x axis at $y = 0$.

$(\Psi_1, \Psi_2)^T$. In the weak interaction limit, the condensates in a rotating frame with angular velocity Ω around the z axis can be well described by the coupled Gross–Pitaevskii equations (CGPEs):

$$i\hbar \frac{\partial \Psi_j(\mathbf{r}, t)}{\partial t} = \left[-\frac{\hbar^2 \nabla^2}{2m} + V + \sum_{k=1}^2 U_{jk} |\Psi_k|^2 - \Omega \hat{L}_z \right] \Psi_j(\mathbf{r}, t), \quad (2)$$

where $U_{jk} = 4\pi \hbar^2 a_{jk}/m$, ($j, k = 1, 2$) represents the intra- (U_{11}, U_{22}) or inter-component (U_{12}) interaction strength characterized by the s -wave scattering length a_{jk} and particle mass m . $\hat{L}_z = -i\hbar(x\partial_y - y\partial_x)$ is the z -component of the angular momentum operator. The wavefunctions are normalized as $\sum_j \int |\Psi_j|^2 d\mathbf{r} = N$, where N is the total number of particles in the condensates.

We can separate the degrees of freedom of the wavefunction as $\Psi_j(\mathbf{r}, t) = \psi_j(x, y, t)\phi(z)$. After rescaling $\tilde{\mathbf{r}} = \mathbf{r}/a_0$, $\tilde{t} = \omega_{\perp} t$, $\tilde{\psi}_j = \psi_j a_0 / \sqrt{N}$, $\tilde{\Omega} = \Omega/\omega_{\perp}$, $\tilde{L}_z = L_z/\hbar$, where $a_0 = \sqrt{\hbar/m\omega_{\perp}}$, we obtain the two-dimensional dimensionless coupled CGPEs (for simplicity, we remark \bullet instead of $\tilde{\bullet}$ in the following):

$$i \frac{\partial \psi_1}{\partial t} = \left(-\frac{1}{2} \nabla^2 + \frac{1}{2} V_0(r - r_0)^2 \right) \psi_1 + g_{11} |\psi_1|^2 + g_{12} |\psi_2|^2 - \Omega L_z \psi_1, \quad (3a)$$

$$i \frac{\partial \psi_2}{\partial t} = \left(-\frac{1}{2} \nabla^2 + \frac{1}{2} V_0(r - r_0)^2 \right) \psi_2 + g_{22} |\psi_2|^2 + g_{12} |\psi_1|^2 - \Omega L_z \psi_2, \quad (3b)$$

where the interaction coefficients are defined as $g_{jk} = 4\pi N \eta a_{jk}$ with the reductive parameter $\eta = \int dz |\phi(z)|^4 / \int dz |\phi(z)|^2$, and the wavefunctions are normalized as $\sum_j \int |\psi_j|^2 dx dy = 1$. Considering the added centrifugal potential when $\Omega \neq 0$, we assume $\Omega^2 < V_0$ in the following in order to ensure that the condensates can be trapped.

In addition, we assume that the particle distribution satisfies the relation:

$$\int (|\psi_1|^2 - |\psi_2|^2) d\mathbf{r} = M, \quad (4)$$

where $M \in (0, 1)$ is an adjustable parameter representing the distribution of particles in two components, assuming the

particle distribution of the first component is larger than that of the second component.

3. Two-component miscible BECs

In this section, we consider the two-component miscible BECs trapped in an annular potential. Their interaction coefficients satisfy $g_{12}^2 < g_{11}g_{22}$. We can give an equivalent Lagrangian formalism based on the GPEs

$$\mathcal{L}[\psi_1, \psi_2] = \mathcal{T}[\psi_1, \psi_2] - \mathcal{F}[\psi_1, \psi_2] \quad (5)$$

where

$$\mathcal{T}[\psi_1, \psi_2] = \int d\mathbf{r} \left\{ \sum_{j=1,2} \left[\frac{i}{2} \left(\psi_j^* \frac{\partial \psi_j}{\partial t} - \frac{\partial \psi_j^*}{\partial t} \psi_j \right) \right] \right\} \quad (6)$$

is the time-dependent part of the Lagrangian functional, and

$$\mathcal{F}[\psi_1, \psi_2] = \int d\mathbf{r} \left\{ \sum_{j=1,2} \left[\frac{1}{2} |\nabla \psi_j|^2 + V |\psi_j|^2 + \sum_{k=1,2} \frac{g_{jk}}{2} |\psi_j|^2 |\psi_k|^2 - \Omega \operatorname{Re} (\psi_j^* L_z \psi_j) - \mu_j |\psi_j|^2 \right] \right\} \quad (7)$$

is the free-energy functional, and μ_j is a Lagrangian multiplier.

3.1. TF approximation

Using the replacement $\psi_j = \sqrt{\rho_j(\mathbf{r}, t)} \exp(i\theta_j(\mathbf{r}, t))$, we obtain $|\nabla \psi_j|^2 = |\nabla \sqrt{\rho_j}|^2 + |\nabla \theta_j|^2 |\psi_j|^2$ in equation (7). The absolute squared amplitude $\rho_j(\mathbf{r}, t) = |\psi_j(\mathbf{r}, t)|^2$ gives the condensate density and the gradient of the phase $\theta_j(\mathbf{r}, t)$ gives the dimensionless superfluid velocity $\mathbf{v} = \nabla \theta_j(\mathbf{r}, t)$ of the j th component. In particular, as the trap structure can be changed conveniently by adjusting the parameters V_0 and r_0 , a density hole might appear in one or both components. So the density distribution of each component may be a disc or an annulus. Whether it is a disc or an annulus, $\mathbf{v} = \boldsymbol{\Omega} \times \mathbf{r}$, is always valid [20, 15]. The curvature of the density $\nabla \sqrt{\rho_j}$ is neglected in the TFA. In this approximation, the variation of the free energy $\mathcal{F}[\psi_1, \psi_2]$ with respect to $|\psi_j|^2$ yields

$$g_{11}|\psi_1|^2 + g_{12}|\psi_2|^2 = \mu_1 + \frac{1}{2}\Omega^2 r^2 - V, \quad (8a)$$

$$g_{22}|\psi_2|^2 + g_{12}|\psi_1|^2 = \mu_2 + \frac{1}{2}\Omega^2 r^2 - V, \quad (8b)$$

and these two coupled equations yield the TF densities of two components

$$\rho_1(\mathbf{r}) = \frac{(g_{22} - g_{12})[(\Omega^2 - V_0)r^2 + 2r_0V_0r - r_0^2V_0]}{2(g_{11}g_{22} - g_{12}^2)} + \frac{g_{22}\mu_1 - g_{12}\mu_2}{(g_{11}g_{22} - g_{12}^2)}, \quad (9a)$$

$$\rho_2(\mathbf{r}) = \frac{(g_{11} - g_{12})[(\Omega^2 - V_0)r^2 + 2r_0V_0r - r_0^2V_0]}{2(g_{11}g_{22} - g_{12}^2)} + \frac{g_{11}\mu_2 - g_{12}\mu_1}{(g_{11}g_{22} - g_{12}^2)}, \quad (9b)$$

for $\rho_j(\mathbf{r}) > 0$ and $\rho_j(\mathbf{r}) = 0$ otherwise. It is difficult to present an explicit expression of the chemical potentials μ_1 and μ_2 , but they can be determined by the normalization condition and equation (4).

3.2. Condensate with a central hole

We assume that two components have no central hole initially, i.e. the density profiles of two components are disc shaped when $\Omega = 0$. With increasing Ω , a central hole will appear in one or both components because of the strong Coriolis forces, and the density profiles will change from disc to annulus. The TF radius R_j of the j th component can be obtained by finding where the density goes to zero. Then we obtain

$$R_1^\pm = \frac{V_0 r_0 \pm \sqrt{\Omega^2 V_0 r_0^2 + (V_0 - \Omega^2) \frac{2(g_{22}\mu_1 - g_{12}\mu_2)}{(g_{22} - g_{12})}}}{(V_0 - \Omega^2)}, \quad (10a)$$

$$R_2^\pm = \frac{V_0 r_0 \pm \sqrt{\Omega^2 V_0 r_0^2 + (V_0 - \Omega^2) \frac{2(g_{11}\mu_2 - g_{12}\mu_1)}{(g_{11} - g_{12})}}}{(V_0 - \Omega^2)}. \quad (10b)$$

Here the plus sign denotes the outer radius R_j^+ and the minus sign denotes the inner radius R_j^- of the annulus of the j th component. A central hole first appeared in the first component when the chemical potentials satisfy the relation $g_{22}\mu_1 - g_{12}\mu_2 = \frac{V_0 r_0^2}{2} (g_{22} - g_{12})$. Substituting it into equation (10a), we obtain the corresponding TF radii $R_1^+ = \frac{2V_0 r_0}{(V_0 - \Omega^2)}$ and $R_1^- = 0$. According to the normalization condition and equation (4), we obtain the critical angular velocity of the first component satisfying

$$\Omega_{1h}^2 = V_0 \left\{ 1 - \left[\frac{8V_0 r_0^4 \pi (g_{22} - g_{12})}{3(1+M)(g_{11}g_{22} - g_{12}^2)} \right]^{1/3} \right\}. \quad (11)$$

Similarly, we obtain the critical angular velocity of the second component satisfying

$$\Omega_{2h}^2 = V_0 \left\{ 1 - \left[\frac{8V_0 r_0^4 \pi (g_{11} - g_{12})}{3(1-M)(g_{11}g_{22} - g_{12}^2)} \right]^{1/3} \right\}, \quad (12)$$

where the chemical potentials satisfy $g_{11}\mu_2 - g_{12}\mu_1 = \frac{V_0 r_0^2}{2} (g_{11} - g_{12})$, and the TF radii of the second component is $R_2^+ = \frac{2V_0 r_0}{(V_0 - \Omega^2)}$ and $R_2^- = 0$.

From equations (10a) and (10b) we can see that the TF inner and outer radii of the annulus of each component satisfy the simple relation

$$R_j^+ + R_j^- = \frac{2V_0 r_0}{(V_0 - \Omega^2)}. \quad (13)$$

This equation shows that the mean radius is determined by V_0 , r_0 and Ω . It grows with increasing angular frequency, increasing r_0 and decreasing V_0 .

With rotation, three density patterns of the condensates can be classified without considering the single vortex in the condensates. Without loss of generality, we assume that $\Omega_{1h} > \Omega_{2h}$; then the central hole firstly appears in the second component when we increase the rotation frequency.

Case 1: $\Omega < \Omega_{2h} < \Omega_{1h}$. Both components are disc shaped, and their TF radii are R_1^+ and R_2^+ in equation (10).

Case 2: $\Omega_{2h} < \Omega < \Omega_{1h}$. The first component is disc shaped and the second component is annulus shaped, and their TF radii are R_1^+ and R_2^\pm in equation (10). A giant vortex is formed in the second component.

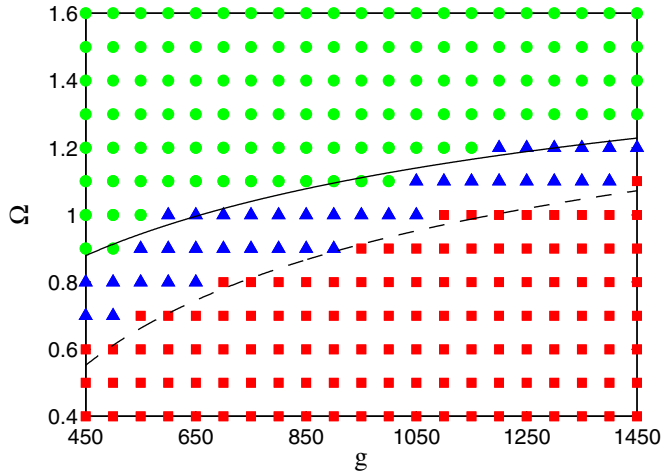


Figure 2. Ω - g phase diagram for parameters $g_{12} = 400$, $V_0 = 4$, $r_0 = 2$ and $M = 0.2$. The squares indicate that two components are disc shaped, the triangles indicate that the big component is a disc and the small component is an annulus, and the circles indicate that two components are annulus shaped. The solid line indicates the critical angular velocity of the big component from equation (11), and the dashed line indicates the critical angular velocity of the small component from equation (12).

Case 3: $\Omega_{2h} < \Omega_{1h} < \Omega$. Both components are annulus shaped and their TF radii are R_1^\pm and R_2^\pm in equation (10), respectively. A giant vortex is formed in each component.

Assuming $g_{11} = g_{22} = g$, we illustrate the phase diagram of the ground-state density distribution of the two components with the varied Ω and g . Other parameters of the system are assumed as $g_{12} = 400$, $V_0 = 4$, $r_0 = 2$ and $M = 0.2$ in our simulations. By using the imaginary-time propagation method $t \rightarrow \tau = it$ [21, 22], we solve equations (3a) and (3b) numerically and obtain a series of ground states of the condensates, as shown in figure 2. We also show the relationship between the critical angular velocity Ω_{jh} of the j th component and g obtained from equations (11) and (12) in figure 2. The results from the numerical simulation and the analytic calculation show good agreement.

In addition, the central hole(s) might also appear as Ω is absent with the suitable values of V_0 and r_0 . Using the above methods, we can also obtain the critical value of V_0 for the appearance of a central hole

$$V_0^{1h} = \frac{3(1+M)(g_{11}g_{22} - g_{12}^2)}{8\pi r_0^4 (g_{22} - g_{12})}. \quad (14a)$$

$$V_0^{2h} = \frac{3(1-M)(g_{11}g_{22} - g_{12}^2)}{8\pi r_0^4 (g_{11} - g_{12})}. \quad (14b)$$

Assuming $V_0^{1h} > V_0^{2h}$, the density patterns of the condensates corresponding to the above cases 1–3 are determined by $V_0 < V_0^{2h} < V_0^{1h}$, $V_0^{2h} < V_0 < V_0^{1h}$ and $V_0^{1h} < V_0^{2h} < V_0$, respectively. And we can obtain the TF radii when we let $\Omega = 0$ in equations (10a) and (10b). Then equation (13) becomes $R_j^+ + R_j^- = 2r_0$. It means that the mean radius of the annular component is only determined by r_0 . So the j th component

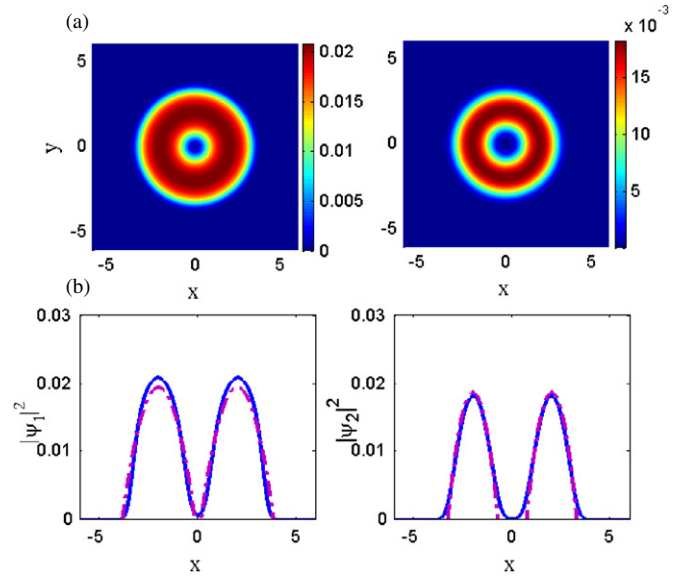


Figure 3. (a) The ground state density profiles of $|\psi_1|^2$ (left) and $|\psi_2|^2$ (right) for $\Omega = 0$ and $V_0 = 25$. (b) The cross sections of $|\psi_1|^2$ (left) and $|\psi_2|^2$ (right) along the x axis at $y = 0$, where solid and dashed curves represent the results obtained from the numerical calculation and those obtained from the analytical calculation in TF approximation respectively.

has a constant mean radius for different V_0 ($V_0 > V_0^{jh}$), if it is annular shaped, and two components have the same mean radius r_0 , if they are both annular shaped.

We take an example for comparing the analytical calculations with numerical simulations when $\Omega = 0$. The intra- and inter-component interactions of the condensates are chosen $g_{11} = 1000$, $g_{22} = 800$ and $g_{12} = 600$. We assume $r_0 = 2$, $M = 0.2$ and $V_0 = 25$. From equations (14a) and (14b), we obtain the critical values $V_0^{1h} = 19.7$, $V_0^{2h} = 6.6$. As V_0 satisfies $V_0^{2h} < V_0^{1h} < V_0$, the density profiles of both components are annulus shaped, as shown in figure 3. The density distribution of two components shows the local minimum at $r = 0$ and the local maximum at $r = 2$. According to equations (10a) and (10b) with $\Omega = 0$, the TF radii of two components are $R_1 = 3.85$ and $R_2 = 0.15$. Figure 3(b) shows the cross sections of $|\psi_1|^2$ and $|\psi_2|^2$ along the x axis at $y = 0$, where solid and dashed curves represent the results obtained from the numerical calculation and the variational calculation, respectively.

It should be emphasized that the TF approximation assumes that the healing length ξ is much smaller than the width of the annulus, where $\xi_j = \hbar/\sqrt{2mg_j\rho_j}$, characterizing the vortex core size of a j th component BEC. In addition, the central hole in our paper means a zero density region at the trap centre when Ω is absent. For the case that $\Omega \neq 0$, several vortices will appear due to the nonzero angular momentum; then the central hole in our paper does not mean a single quantized vortex in the trap centre, but a giant vortex, i.e. a vortex with multiple quantum circulation.

4. Two-component immiscible BECs

4.1. TF approximation for the case of $N_1 \gg N_2$

In this section, we assume that the inter-component scattering length is larger than the intra-component scattering length. Then the two components are immiscible, and the TFA is no longer applicable because the TFA fails to describe the domain boundary region, where the quantum pressure term cannot be neglected. But if $N_1 \gg N_2$, the density distribution of the big component is hardly affected by the small component, and the small component experiences a trap not only produced by the external trap but also by the repulsive interaction of the big component. So we can respectively approximate their profiles with the TF distribution.

For the big component, the TF density is

$$\rho_1(r) = \frac{\mu_1 - \frac{1}{2}[V_0(r-r_0)^2 - \Omega^2 r^2]}{g_{11}}, \quad (15)$$

for $\rho_1(\mathbf{r}) > 0$ and $\rho_1(\mathbf{r}) = 0$ otherwise. The chemical potential μ_1 can be determined by the normalization condition $\int |\psi_1|^2 d\mathbf{r} = 1$. Its effective potential is $V_{\text{eff1}} = [V_0(r-r_0)^2 - \Omega^2 r^2]/2$, and we define $V_{\text{eff1}}^0 = \frac{1}{2}V_0 r_0^2$, representing the value of the effective potential at $r = 0$. With the angular frequency increasing, a central hole will appear. According to the normalization condition, we obtain the square of critical angular frequency

$$\Omega_{1h}^2 = V_0 \left[1 - \left(\frac{4\pi V_0 r_0^4}{3g_{11}} \right)^{1/3} \right]. \quad (16)$$

When $\Omega = \Omega_{1h}$, the TF radius is $R_1 = \frac{2V_0 r_0}{(V_0 - \Omega^2)}$ and the chemical potential $\mu_1 = V_{\text{eff1}}^0$. For $\Omega < \Omega_{1h}$, the density distribution of the big component is a disc. Its TF radius is

$$R_1 = \frac{V_0 r_0 + \sqrt{V_0 r_0^2 \Omega^2 + 2\mu_1(V_0 - \Omega^2)}}{V_0 - \Omega^2}. \quad (17)$$

For $\Omega > \Omega_{1h}$, the density profile of the big component is an annulus. Its TF inner and outer radii are

$$R_1^\pm = \frac{V_0 r_0}{(V_0 - \Omega^2)} \pm \left(\frac{3g_{11}}{4\pi r_0 V_0} \right)^{1/3}, \quad (18)$$

where the plus sign denotes the outer radius R_1^+ and the minus sign denotes the inner radius R_1^- . The chemical potential $\mu_1 = \frac{(6g_{11}V_0^2 r_0^2 \pi^2)^{2/3}(V_0 - \Omega^2)}{8r_0^2 \pi^2 V_0^2} - \frac{r_0^2 V_0 \Omega^2}{2(V_0 - \Omega^2)} < V_{\text{eff1}}^0$. And the inner and outer radii satisfy the relation

$$R_1^+ + R_1^- = \frac{V_0 r_0}{(V_0 - \Omega^2)}, \quad R_1^+ - R_1^- = \left(\frac{6g_{11}}{\pi r_0 V_0} \right)^{1/3}. \quad (19)$$

From equation (19) we can see that the mean radius is only determined by the potential and the rotation frequency, which is similar to the case of two-component miscible condensates. And the width of the annulus is unrelated to the rotation frequency. In other words, if we increase the rotation frequency, the inner and outer radii will increase due to the stronger centrifugal force, but the width of the annulus is unchanged. In addition, when $\Omega = 0$, the central hole might also appear, and the critical value of V_0 is $V_0^h = \frac{3g_{11}}{4\pi r_0^4}$. For $V_0 > V_0^h$, the condensate is annulus shaped, and for $V_0 < V_0^h$,

the condensate is disc shaped. It should be pointed out that the above conclusions in this section also apply to the case of a single-component BEC in this trap.

For the small component, the situation is more complicated. Its density distribution is not only affected by the external potential, but also by the big component. The effective potential of the small component is $V_{\text{eff2}} = \frac{V_0}{2}(r-r_0)^2 + g_{12}\rho_1 - \frac{\Omega^2 r^2}{2}$. According to the density profiles of the big component, and the competition among the chemical potentials and the effective potential barriers of the two components, the density profile of the small component can be divided into the following three cases.

Case 1. The density profile of the big component is a disc and that of the small component is an annulus surrounding the big component. In this case, the chemical potentials and the effective potentials at $r = 0$ satisfy $V_{\text{eff1}}^0 < \mu_2 < \mu_1 < V_{\text{eff2}}^0$; here $V_{\text{eff2}}^0 = \left(\mu_1 - \frac{V_0 r_0^2}{2} \right) g_{12}/g_{11} + \frac{V_0 r_0^2}{2}$. The TF radii of the annulus are

$$R_2^- = \frac{V_0 r_0 + \sqrt{V_0 r_0^2 \Omega^2 - 2(V_0 - \Omega^2) \frac{g_{11}\mu_2 - g_{12}\mu_1}{g_{12} - g_{11}}}}{V_0 - \Omega^2} \quad (20)$$

$$R_2^+ = \frac{V_0 r_0 + \sqrt{V_0 r_0^2 \Omega^2 + 2\mu_2(V_0 - \Omega^2)}}{V_0 - \Omega^2}. \quad (21)$$

Case 2. The density profile of the big component is an annulus and that of the small component is a small disc plus a big annulus. The small disc fills the density hole of the big component and the big annulus surrounds the big component. There is a local maximum value of the effective potential $V_{\text{eff2}} = \frac{V_0 r_0^2}{2}$ at $r = 0$, and a local minimum value $V_{\text{eff2}} = \mu_1$ at $r = R_1$. In this situation, $\mu_1 < V_{\text{eff1}}^0 = V_{\text{eff2}}^0 < \mu_2$; here, $V_{\text{eff2}}^0 = \frac{V_0 r_0^2}{2}$. The corresponding TF radius of the disc is

$$R_2^{\text{disc}} = \frac{V_0 r_0 - \sqrt{V_0 r_0^2 \Omega^2 - 2(V_0 - \Omega^2) \frac{g_{11}\mu_2 - g_{12}\mu_1}{g_{12} - g_{11}}}}{V_0 - \Omega^2}, \quad (22)$$

and the TF radii of the annulus can be obtained by equations (20) and (21).

Case 3. The density profile of the big component is an annulus and that of the small component is a small annulus plus a big annulus. The small annulus of the small component is surrounded by the big component, and the big annulus of the small component surrounds the big component. In this case, $\mu_1 < \mu_2 < V_{\text{eff1}}^0 = V_{\text{eff2}}^0$; here, $V_{\text{eff2}}^0 = \frac{V_0 r_0^2}{2}$. The corresponding TF radii are

$$R_{2s}^- = \frac{V_0 r_0 - \sqrt{2\mu_2(V_0 - \Omega^2) + V_0 r_0^2 \Omega^2}}{V_0 - \Omega^2}, \quad (23a)$$

$$R_{2s}^+ = \frac{V_0 r_0 - \sqrt{\Omega^2 V_0 r_0^2 - 2(V_0 - \Omega^2) \frac{g_{11}\mu_2 - g_{12}\mu_1}{g_{12} - g_{11}}}}{V_0 - \Omega^2}, \quad (23b)$$

$$R_{2b}^- = \frac{V_0 r_0 + \sqrt{\Omega^2 V_0 r_0^2 - 2(V_0 - \Omega^2) \frac{g_{11}\mu_2 - g_{12}\mu_1}{g_{12} - g_{11}}}}{V_0 - \Omega^2}, \quad (23c)$$

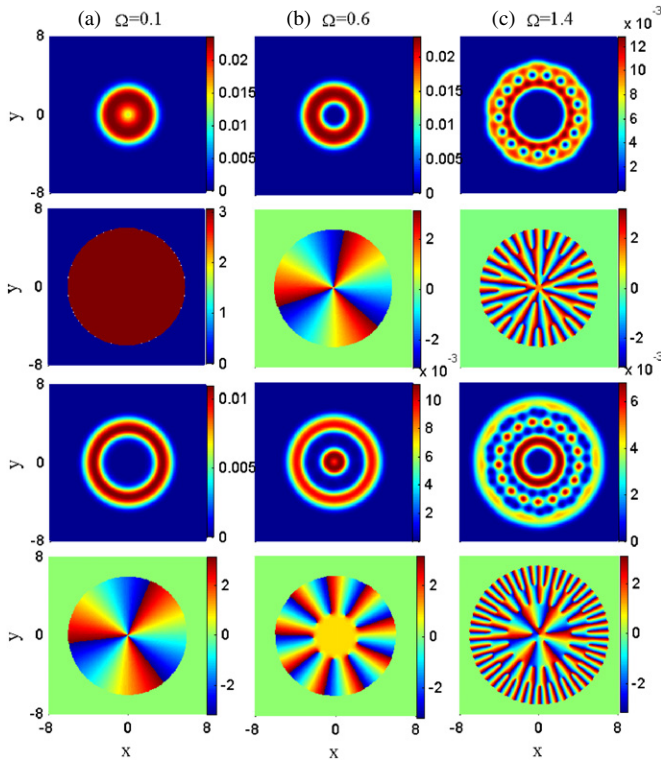


Figure 4. The ground state density profiles and phases for different angular velocities: (a) $\Omega = 0.1\omega_{\perp}$, (b) $\Omega = 0.6\omega_{\perp}$ and (c) $\Omega = 1.4\omega_{\perp}$. The first and the third rows are the density profiles of ψ_1 and ψ_2 . The second and the fourth rows are the phases corresponding to the density profiles of the first and the third rows, respectively.

$$R_{2b}^+ = \frac{V_0 r_0 + \sqrt{2\mu_2(V_0 - \Omega^2) + V_0 r_0^2 \Omega^2}}{V_0 - \Omega^2}, \quad (23d)$$

where R_{2s}^- and R_{2s}^+ represent the inner and outer radii of the small annulus, and R_{2b}^- , R_{2b}^+ represent the inner and outer radii of the big annulus, respectively. It should be emphasized that we only consider the condensates with a symmetrical structure in this paper. In other words, we do not consider the case that the condensates have broken symmetry; for example, the centre of two components differ or the condensates are two droplets [19].

4.2. Spin textures

In this section, we discuss three kinds of spin textures of the two-component immiscible BECs with different angular velocities Ω . The intra- and inter-component interactions of the condensates and other parameters are chosen $g_{11} = 550$, $g_{22} = 1000$, $g_{12} = 800$, $M = 0.2$, $V_0 = 4$, $r_0 = 2$. The density profiles and corresponding phases are shown in figure 4. The big component locates near the trap centre, and the small component spreads to the low density region of the big component because of its strong intra-component interaction. When $\Omega = 0.1\omega_{\perp}$, the density profile of the big component is a disc and that of the small component is an annulus, as shown in figure 4(a). Three phase defects of the small component enter into the centre density hole,

forming a giant vortex. The spinor-order parameter of the two-component BECs allows us to analyse this system as a pseudospin-1/2 BEC [23]. We introduce a normalized complex valued spinor $\chi = [\chi_1(\mathbf{r}), \chi_2(\mathbf{r})]^T = [|\chi_1|e^{i\theta_1}, |\chi_2|e^{i\theta_2}]^T$, which satisfies $|\chi_1|^2 + |\chi_2|^2 = 1$. Then the wavefunctions are decomposed as $\psi_j = \sqrt{\rho_T(\mathbf{r})}\chi_j(\mathbf{r})$. The pseudospin density is defined as $S = \bar{\chi}(\mathbf{r})\sigma\chi(\mathbf{r})$; here, σ is the Pauli matrix. The pseudospin density is expressed as

$$\begin{cases} S_x = 2|\chi_1||\chi_2|\cos(\theta_1 - \theta_2), \\ S_y = -2|\chi_1||\chi_2|\sin(\theta_1 - \theta_2), \\ S_z = |\chi_1|^2 - |\chi_2|^2, \end{cases} \quad (24)$$

and $|S| = \sqrt{S_x^2 + S_y^2 + S_z^2} = 1$. Projecting the system into a pseudospin space, the spin of the big component points up, and the spin of the small component points down. The pseudospin twists through an angle of π from up to down continuously between two components. Figure 5 shows the pseudospin textures about the case of figure 4(a). The corresponding pseudospin texture is a giant skyrmion. The topological charge Q of the giant skyrmion is equal to the quantum of circulation of the giant vortex, where the topological charge is $Q = \int d\mathbf{r}q(\mathbf{r})$ [24], and the topological charge density $q(\mathbf{r}) = \frac{1}{8\pi}\epsilon^{ij}\mathbf{S} \cdot \partial_i\mathbf{S} \times \partial_j\mathbf{S}$ characterizes the spatial distribution of the skyrmion. In this case, the spatial distribution of the topological charge density is an annulus, as shown in figure 5(c), which is located at the interface of the two components. This spin texture has been observed and studied in a harmonic potential [18].

In this section, we mainly study another case that the density profile of the big component is annulus shaped. With the increase of the angular velocity, e.g. $\Omega = 0.6\omega_{\perp}$, the density profile of the big component becomes an annulus due to the strong centrifugal effect, and the density profile of the small component develops into a disc plus an annulus, as shown in figure 4(b). The big component forms a density hole which creates a giant vortex with quantum number 3 of circulation, and there are nine single quantized vortices distributed in the annular no-density areas of the small component. In the pseudospin space, a new spin texture is formed, and we name it concentric double-annulus skyrmion. The corresponding pseudospin densities S_x and S_z are presented in figures 6(a) and (b). The topological charge density is uniformly distributed at two concentric-annulus regions where the two immiscible condensates overlap, as shown in figure 6(c). The projected vectorial plots of (S_x, S_y) are shown in figures 6(d) and (e). This new spin texture can be regarded as the combination of two annular (giant) skyrmions.

In the polar coordinates, the phases of two components can approximately be written as $\theta_j = \kappa_j\phi$, where $\kappa_j = 0, 1, 2, \dots$ represents the quantum number of the circulation of the j th component restricted in a radius r . Then the pseudospin density can be rewritten as

$$\begin{cases} S_x = \sqrt{1 - [S_z(r)]^2} \cos[(\kappa_1 - \kappa_2)\phi], \\ S_y = \sqrt{1 - [S_z(r)]^2} \sin[(\kappa_1 - \kappa_2)\phi], \\ S_z = S_z(r), \end{cases} \quad (25)$$

and the corresponding topological charge density can be expressed as

$$q(\mathbf{r}) = \frac{[\kappa_1 - \kappa_2]}{4\pi r} \frac{dS_z(r)}{dr}. \quad (26)$$

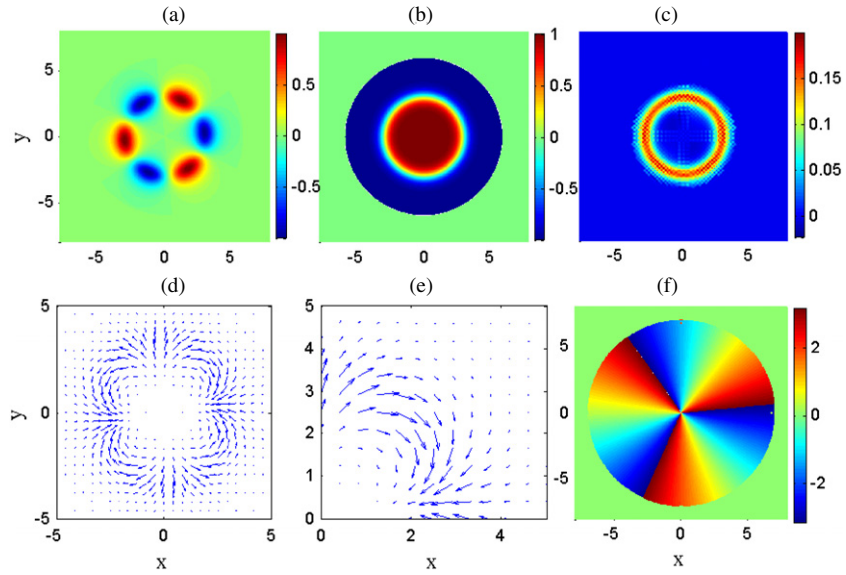


Figure 5. The pseudospin densities distribution for (a) S_x , (b) S_z with $\Omega = 0.1\omega_{\perp}$. (c) The distribution of the topological charge density $q(\mathbf{r})$. (d) The vectorial representation of the spin texture projected onto the x - y plane, and (e) an amplified local part of (d). (f) The relative phase $\theta_1 - \theta_2$.

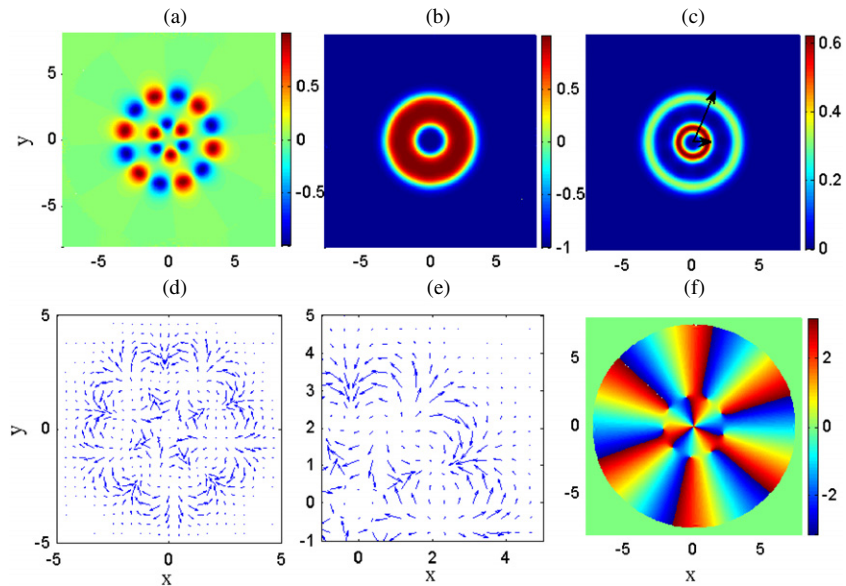


Figure 6. The pseudospin densities distribution for (a) S_x , (b) S_z with $\Omega = 0.6\omega_{\perp}$. (c) The distribution of the topological charge density $q(\mathbf{r})$. The length of the long (short) arrow indicates the outer radius d_1 (d_2) of the bigger (smaller) annular skyrmion. (d) The vectorial representation of the spin texture projected onto the x - y plane, and (e) an amplified local part of (d). (f) The relative phase $\theta_1 - \theta_2$.

Figure 4(b) shows $\kappa_1 = 3$, $\kappa_2 = 0$, when $r = d_1$, and $\kappa_1 = 3$, $\kappa_2 = 9$, when $r = d_2$, where d_1 and d_2 are the outer radii of two annular skyrmions, as shown in figure 6(c). So the topological charges of the skyrmions in figure 6 are

$$\begin{aligned}
 Q_i &= \int \frac{(\kappa_1 - \kappa_2)_i}{4\pi r} \frac{dS_z(r)}{dr} \mathbf{dr} \\
 &= \frac{(\kappa_1 - \kappa_2)_i}{2} [S_z(d_1) - S_z(0)] \\
 &= (\kappa_1 - \kappa_2)_i = 3,
 \end{aligned} \tag{27}$$

$$\begin{aligned}
 Q_o &= \frac{(\kappa_1 - \kappa_2)_o}{2} [S_z(d_2) - S_z(d_1)] \\
 &= -(\kappa_1 - \kappa_2)_o = 6,
 \end{aligned} \tag{28}$$

$$Q_c = Q_i + Q_o = 9, \tag{29}$$

where Q_i , Q_o and Q_c represent the topological charge of the inner annular skyrmion, that of the outer annular skyrmion and the total topological charge of the concentric double-annulus skyrmion, respectively. It can be summarized as follows: the topological charge of each annular skyrmion is equal to the absolute value of the difference between the quantum number of circulation of two components surrounded in this skyrmion, as shown in figure 6(f), and the topological charge of the concentric double-annulus skyrmion is the sum of the one of two annular skyrmions.

As the angular velocity increases further, e.g. $\Omega = 1.4\omega_{\perp}$, some single quantized vortices appear at the density region

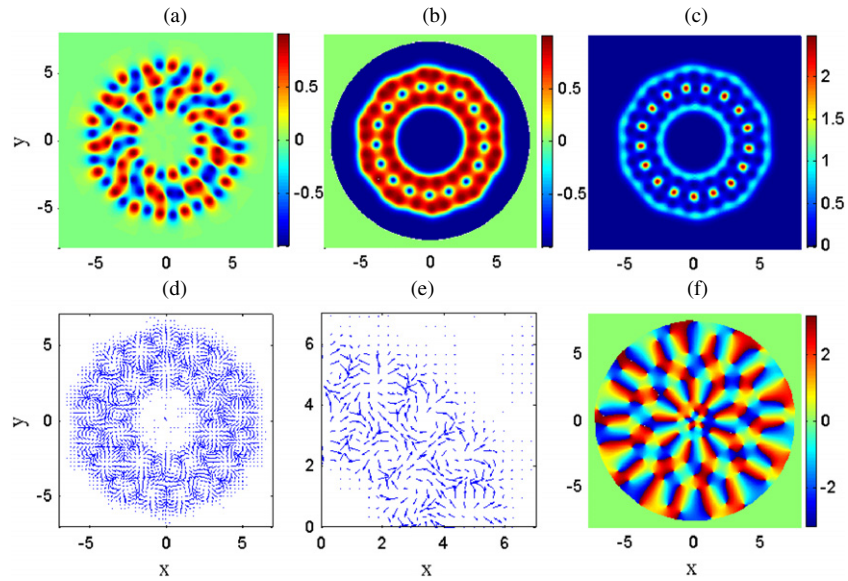


Figure 7. The pseudospin densities distribution for (a) S_x , (b) S_z with $\Omega = 1.4\omega_{\perp}$. (c) The distribution of the topological charge density $q(\mathbf{r})$. (d) The vectorial representation of the spin texture projected onto the x - y plane, and (e) an amplified local part of (d). (f) The relative phase $\theta_1 - \theta_2$.

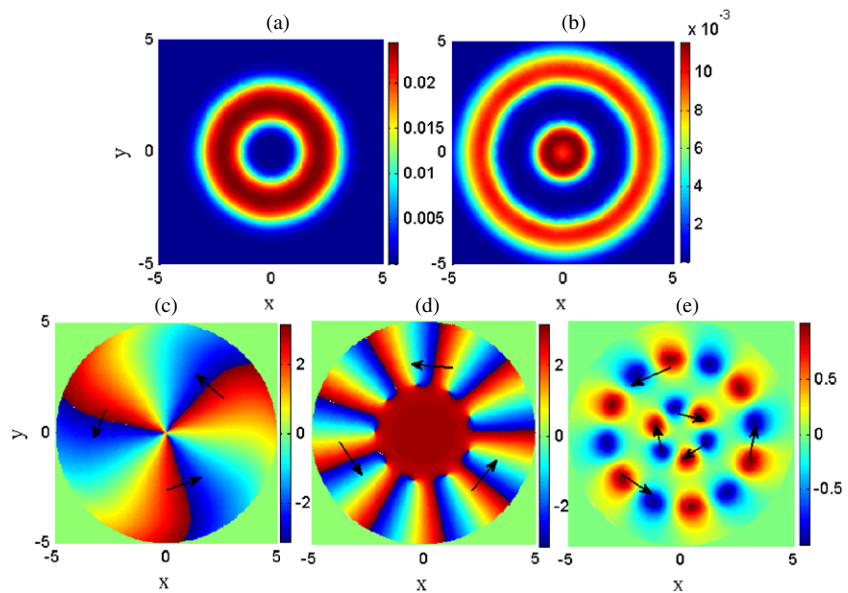


Figure 8. The density profiles of (a) ψ_1 and (b) ψ_2 of the real time dynamical evolution at $t = 30\omega_{\perp}^{-1}$ with the same parameters as figure 4(b). (c), (d) The corresponding phases of (a) and (b). (e) The pseudospin density distribution of S_x . The rows indicate the rotational direction.

of the big component, and these vortices are filled with the density of the small component, forming some coreless vortices without a density dip in the total density, as shown in figure 4(c). Projecting the system into a pseudospin space, many skyrmions are embedded in the concentric double-annulus skyrmion, as shown in figure 7. The topological charge for each embedded skyrmion is equal to 1. And the topological charge densities of these embedded skyrmions are distributed on a ring and show a δ -function distribution. For the concentric double-annulus skyrmion, the topological charge of each annular skyrmion is also equal to the absolute value of the difference between the quantum number of circulation of two components inside this skyrmion.

4.3. Dynamical behaviours under external disturbances

In this section, we investigate the dynamical behaviours of two immiscible BECs under an external disturbance. We choose the ground state obtained in figure 4(c) as an initial value and perform real time dynamic evolutions of equation (3a) by introducing a small disturbance such as a Gaussian beam $V_{\text{beam}} = 0.5e^{-[(x-4)^2+y^2]/0.5}$ for the interval $t = [0, 1.5\omega_{\perp}^{-1}]$. The density profiles, phases and the pseudospin density S_x at $t = 30\omega_{\perp}^{-1}$ are shown in figure 8. We can see that the density profiles and the spin textures are stable and robust. The vortices in each component generate a collective circular motion, as shown in figures 8(c) and (d). It is easy to understand because the Gaussian disturbance brings small amounts of

energy into the system, and the energy is too small to change the density distribution of condensates, just generating a small surface ripples at the boundary of the condensates. But for the vortices located in the extremely low density regions, the energy is enough to excite their movement. The pseudospin density S_x of the inner annular skyrmion rotates clockwise, and the one of the outer skyrmion rotates anticlockwise, as shown in figure 8(e), because two components distributed inside and outside two annular skyrmions are exchanged. The rotation of S_y is similar to S_x , and S_z is invariable. If we increase the external disturbance, the bigger energy will drive two condensates to rotate reversely to conserve the angular momentum of the system. Finally it should be indicated that the spin textures presented above are still stable and robust in a slightly inhomogeneous trap.

5. Conclusion

We have studied analytically and numerically the ground states of the miscible two-component BECs with or without rotation based on the TFA. With rotation, we have analytically obtained the critical angular velocity for a central hole to appear in each condensate and present the phase diagram which shows three kinds of density profiles of the ground states by varying the angular velocities and intra-component interaction strengths. Without rotation, we have also classified the density profiles according to different potential barriers. In addition, we have discussed the immiscible two-components BECs for the case of $N_1 \gg N_2$ with the TFA. We give the critical angular velocity for a central hole to appear in the big condensate, and classify its density profiles according to different angular velocity. We find that the width of the density annulus of the big component is unchanged for different rotation angular velocity. And the density profile of the big component is almost the same whether the small component exists or not, so the conclusion of the big component in this situation is still valid for the single-component BEC. Three kinds of density profiles of the condensates have been classified according to the competition among the chemical potentials and the effective potential barriers.

We have obtained three kinds of spin textures for the immiscible two-component BECs: annular skyrmion (giant skyrmion), concentric double-annulus skyrmion and a concentric double-annulus skyrmion with an embedded skyrmion ring. The annular skyrmion has been observed and studied in the harmonic traps but the last two kinds of spin textures in this paper are new structures and could not be observed in harmonic trapping potentials. Both of the last spin textures contain a concentric double-annulus skyrmion. Its topological charge is the sum of the ones of two annular skyrmions, and the topological charge of each annular skyrmion is equal to the absolute value of the difference between the quantum number of circulation of two components inside this annular skyrmion. We have also studied the dynamical behaviours of the condensates under external disturbance and proved that the spin textures in our paper are robust under a small external disturbance or a slight trap inhomogeneity. We have theoretically predicted these new

robust spin textures in the annular trap and expect that these rich structures would be observed in experiments in the near future.

Acknowledgments

This work was supported by National Natural Science Foundation of China (10972125), Specialized Research Fund for the Doctoral Program of Higher Education of China (20111401110004), Natural Science Foundation of Shanxi Province (2010011001-2) and Project Supported by Shanxi Scholarship Council of China.

References

- [1] Bretin V, Stock S, Seurin Y and Dalibard J 2004 *Phys. Rev. Lett.* **92** 050403
- [2] Ryu C, Andersen M F, Clade P, Natarajan V, Helmerson K and Phillips W D 2007 *Phys. Rev. Lett.* **99** 260401
- [3] Weiler C N, Neely T W, Scherer D R, Bradley A S, Davis M J and Anderson B P 2008 *Nature* **455** 948
- [4] Heathcote W H, Nugent E, Sheard B T and Foot C J 2008 *New J. Phys.* **10** 043012
- [5] Brazhnyi V A, Konotop V V and Kuzmiak V 2004 *Phys. Rev. A* **70** 043604
- [6] Murch K W, Moore K L, Gupta S and Stamper-Kurn D M 2006 *Phys. Rev. Lett.* **96** 013202
- [7] Dutta O, Jääskeläinen M and Meystre P 2006 *Phys. Rev. A* **74** 023609
- [8] Bludov Yu V and Konotop V V 2007 *Phys. Rev. A* **75** 053614
- [9] Abad M, Guilleumas M, Mayol R, Pi M and Jezek D M 2010 *Phys. Rev. A* **81** 043619
- [10] Abad M, Guilleumas M, Mayol R, Pi M and Jezek D M 2011 *Phys. Rev. A* **84** 035601
- [11] Parola A, Salasnich L, Rota R and Reatto L 2005 *Phys. Rev. A* **72** 063612
- [12] Li W, Xie X, Zhan Z and Yang X 2005 *Phys. Rev. A* **72** 043615
- [13] Salasnich L, Parola A and Reatto L 2006 *Phys. Rev. A* **74** 031603
- [14] Tsubota M, Kasamatsu K and Ueda M 2002 *Phys. Rev. A* **65** 023603
Kasamatsu K, Tsubota M and Ueda M 2002 *Phys. Rev. A* **66** 053606
Lundh E 2002 *Phys. Rev. A* **65** 043604
Kavoulakis G M and Baym G 2003 *New J. Phys.* **5** 51
Schweikhard V, Coddington I, Engels P, Mogendorff V P and Cornell E A 2004 *Phys. Rev. Lett.* **92** 040404
Simula T P, Penckwitt A A and Ballagh R J 2004 *Rev. Lett.* **92** 060401
- [15] Kim J K and Fetter A L 2005 *Phys. Rev. A* **72** 023619
- [16] Smyrnakis J, Bargi S, Kavoulakis G M, Magiropoulos M, Kärkkäinen K and Reimann S M 2009 *Phys. Rev. Lett.* **103** 100404
- [17] Shimodaira T, Kishimoto T and Saito H 2010 *Phys. Rev. A* **82** 013647
- [18] Yang S-J, Wu Q-S, Zhang S-N and Feng S 2008 *Phys. Rev. A* **77** 033621
- [19] Mason P and Aftalion A 2011 *Phys. Rev. A* **84** 033611
- [20] Fetter A L, Jackson B and Stringari S 2005 *Phys. Rev. A* **71** 013605
- [21] Dalfovo F and Stringari S 1996 *Phys. Rev. A* **53** 2477
Chiofalo M L, Succi S and Tosi M P 2000 *Phys. Rev. E* **62** 7438
- [22] Bao W, Chern I-L and Lim F Y 2006 *J. Comput. Phys.* **219** 836
- [23] Kasamatsu K, Tsubota M and Ueda M 2005 *Phys. Rev. A* **71** 043611
- [24] Son D T and Stephanov M A 2002 *Phys. Rev. A* **65** 063621